Available online at www.sciencedirect.com
ScienceDirect
C. R. Physique 9 (2008) 524–536
COMPTES RENDUS PHYSIQUE
http://france.elsevier.com/direct/COMREN/

Synchrotron x-rays and condensed matter/Rayonnement X synchrotron et matière condensée

Hard X-ray PhotoEmission Spectroscopy of strongly correlated systems

Giancarlo Panaccione [a,*], Francesco Offi [b], Maurizio Sacchi [c,d], Piero Torelli [e]

[a] *TASC Laboratory, INFM-CNR in Area Science Park, S.S.14, Km 163.5, 34012 Trieste, Italy*
[b] *CNISM and Dipartimento di Fisica Univ. Roma III, Via della Vasca Navale 84, 00146 Roma, Italy*
[c] *Synchrotron SOLEIL, l'orme des merisiers, Saint-Aubin, BP 48, 91192 Gif-sur-Yvette cedex, France*
[d] *Laboratoire de chimie physique-matière et rayonnement (UMR 7614), université Pierre et Marie Curie, 11, rue Pierre et Marie Curie, 75231 Paris cedex 05, France*
[e] *S3, CNR-INFM, Via G. Campi 213/A, 41100 Modena, Italy*

Available online 31 October 2007

Abstract

Hard X-ray PhotoEmission Spectroscopy (HAXPES) is a new tool for the study of bulk electronic properties of solids using synchrotron radiation. We review recent achievements of HAXPES, with particular reference to the VOLPE project, showing that high energy resolution and bulk sensitivity can be obtained at kinetic energies of 6–8 keV. We present also the results of recent studies on strongly correlated materials, such as vanadium sesquioxide and bilayered manganites, revealing the presence of different screening properties in the bulk with respect to the surface. We discuss the relevant experimental features of the metal–insulator transition in these materials. ***To cite this article: G. Panaccione et al., C. R. Physique 9 (2008).***

Résumé

Spectroscopie de photoémission X à haute énergie dans les matériaux fortement corrélés. La spectroscopie de photoémission avec rayons X de haute énergie (Hard X-ray PhotoEmission Spectroscopy, ou HAXPES) est une nouvelle technique qui utilise le rayonnement synchrotron pour l'étude des propriétés électroniques de volume dans les solides. Nous présentons ici les derniers développements du HAXPES, en particulier en ce qui concerne le projet VOLPE, qui montrent que une haute résolution en énergie et une grande sensibilité au volume peuvent être obtenues pour des énergie cinétiques de 6–8 keV. Nous présentons aussi des résultats récents obtenus dans des matériaux fortement corrélés, comme le V_2O_3 et les manganites, qui montrent comment les phénomènes d'écrantage sont différents dans le volume par rapport à la surface. ***Pour citer cet article : G. Panaccione et al., C. R. Physique 9 (2008).***

Keywords: High resolution photoemission; Electron analyser; Correlated systems

Mots-clés : Photoémission à haute résolution ; Analyseur d'électrons ; Systèmes corrélés

* Corresponding author.
E-mail address: panaccioneg@elettra.trieste.it (G. Panaccione).

1631-0705/$ – see front matter
doi:10.1016/j.crhy.2007.04.005

1. Introduction

Since the first experiment performed in the 1950s by Siegbahn (Nobel prize in 1981) and co-workers, Photo-Emission Spectroscopy (PES) (known with different acronyms XPS, ESCA, PES etc.) is one of the most powerful spectroscopic tools to investigate electronic properties. Applications of PES span from geophysics to the study of atoms and clusters, from environmental topics to fundamental research in solid state science. Among the most intriguing systems, and consequently among the most studied, one finds materials with open d and f electron shells, where outer electrons occupy spatially localized orbitals. Electron–electron interaction effects play a dominant role in such materials, often called 'highly correlated electron systems', which include transition metal oxides, lanthanides and actinides [1]. The strong Coulomb repulsion experienced by the electrons and the interplay of the d and f electron internal degrees of freedom—spin, charge, and orbital moment—exhibit many exotic ordering phenomena. Such an interplay makes strongly correlated electron systems extremely sensitive to small changes in external parameters and, consequently, their experimental and analytical study is particularly difficult [1].

As a direct probe of d and f states near the Fermi level (E_F), PES provides important information of immediate interest for refining theoretical models. One can make use of the large energy range covered in PES experiments by studying excitation spectra from several eV up to several hundreds of eV. This provides direct information about the 'bare' electrons, e.g. the charge, spin, and orbital state of the ions that make up the correlated material. By measuring the excitation spectra with high energy resolution in the meV range from the chemical potential, one can find directly the behavior of the 'dressed' electrons, e.g. quasi particles. We would like to stress here that it is not the excitation energy that determines whether the measurement probes the high or low energy scale physics. Instead, it is the observed binding energy and energy resolution with which the measurement is carried out, since this determines the features observed and the quality of the measurement. In fact, the higher the photon energy the better, because the condition for the so-called sudden-approximation is fulfilled better and the spectra represent more directly the imaginary part of the one-hole Green's function, one of the most important quantities in the study of many-body systems. Therefore, low energy scale phenomena are observed when: (i) the measurement is focused on the region near the chemical potential; and (ii) both core level and valence band PES spectra are compared in a controlled manner and with good energy resolution.

An important experimental aspect of PES concerns its probing depth: photoemission is characterised by strong surface sensitivity (<1 nm), an aspect fully exploited in the last four decades for studying the topmost atomic layers in solids and interfaces. However, the electronic structure of the surface is in general very different from the bulk. This was demonstrated, for instance, by the studies of the Laubschat and Kaindl [2,3] and by the group of Suga [4]: using soft-X-rays, thereby increasing the probing depth to about 15 Å, they observed that the valence band spectra of correlated compounds are essentially different from those taken using ultra-violet light. In addition, the presence of vacuum can thermodynamically destabilize the surface affecting local stoichiometry and chemical composition. Therefore, the problem of determining true bulk electronic structure cannot be solved even by measuring a single crystal with a perfect surface termination, since the surface will always have a different electronic structure than the bulk. This is especially true for strongly correlated systems, where small variations of the surrounding of the atomic like 3d, 4f or 5f orbitals has a large impact on the narrow bands. In conclusion, in strongly correlated systems the presence of the surface, i.e. the reduced dimensionality and the broken symmetry that the surface represents, may prevent one from obtaining information on the bulk, leading not only to a more difficult interpretation of experiments but also to a reduced reliability in the comparison with calculations. Recent examples that clearly support this picture can be found in literature [5–7].

In principle, the most straightforward way of increasing bulk sensitivity in PES is to go towards higher values of kinetic energy E_k (6–10 keV), i.e. to perform Hard X-ray PhotoEmission (HAXPES) experiments. Although supported by clear motivations and strong needs, few attempts at developing HAXPES have been made since the pioneering work of Lindau et al. [8]. One first unavoidable drawback is the strong reduction of the photoionization cross section at high photon energy [9]. In this respect, the development of SR sources and of new insertion devices and beamlines delivering high flux, high resolution photon beams in the 10 keV energy range, has considerably improved the experimental conditions with respect to 30 years ago. Successful attempts have been made recently to measure core level and valence band spectra with increased bulk sensitivity thus enabling the use of HAXPES for the study of strongly correlated systems and buried interfaces [10–17]. The objective of such new equipments is to obtain bulk sensitive PES spectra with good statistics and high energy resolution in the range 6–10 keV, to be compared to the results

of standard PES experiments carried out in surface sensitive mode. In this article we present the performances and the main features of a new spectrometer, developed within the VOLPE (VOLume PhotoEmission from solids with Synchrotron Radiation) project, equipped with an electrostatic hemispherical analyser dedicated to HAXPES experiments. The instrument has been successfully tested and is now operational at the European Synchrotron Radiation Facility (ESRF), ID16 beamline. The paper is organized as follows: in Section 2 we review the main technical solution adopted for HAXPES experiments. In Section 3 we discuss the probing depth of the technique. In Section 4 we review some recent results of selected strongly correlated systems. Conclusions and perspectives are drawn in Section 5.

2. Experimental considerations

Performing HAXPES experiments with an energy resolution comparable to what can be obtained in the standard energy range (i.e. $<$100 meV) is, under many aspects, a challenge to present technical capabilities. The lack of a photon source with at the same time high flux and an adequate energy band pass in the range from 2 to 5/6 keV obliges one to perform HAXPES above 5 keV and, as mentioned before, at these kinetic energies the photoionisation cross sections decreases by several orders of magnitude [9,18]. This has important consequences from the point of view of the experimental setup: the electrical insulation of the different elements must be very efficient, the long acquisition times require high stability of the power supplies and of the photon source, the low count rate implies a low noise detection system and the large retarding factor applied to the photoelectrons requires a small electron source point (i.e. a small beam spot size on the sample) and a special design of the electrostatic lens system. In the next sections we will focus on the main technical solutions that have been adopted for the VOLPE project. We remind the reader that an extended and detailed description of the apparatus is reported elsewhere [19].

2.1. Beamline and sample environment

The ID16 beamline has been optimized in the range 6–10 keV with two alternative optical schemes for HAXPES experiments: in both cases, the X-ray beam is pre-monochromatized to a relative bandwidth ($\Delta E/E$) of 1.4×10^{-4} by a Si(111) double-crystal fixed-exit monochromator cooled by a liquid nitrogen closed loop. The pre-monochromatized beam impinges on a Si channel-cut crystal operating at the Si(nnn) reflection (n being 3 at $\approx$6 keV and 4 at $\approx$8 keV) and at a Bragg angle of 88.1°. At the expense of a fixed energy operation, this backscattering geometry allows us to match the source divergence and to obtain a highly monochromatic beam. This optical configuration provides 6.2×10^{11} ph/s with a resolution of 50 meV at 6 keV and 2.6×10^{11} ph/s with 14 meV of resolution at 10 keV. The second optical scheme is based on the use of a set of three channel-cut monochromators [Si(1,1,1), Si(1,1,0) and Si(1,0,0)] which can be operated at several reflection orders depending on the specific requirements of energy, intensity and resolution. Although the energy bandwidth is larger than in backscattering geometry, this latter configuration permits to tune the photon energy continuously over a wide range. A Rh-coated toroidal mirror focuses the beam at the sample position in a spot size of 50×120 μm^2. The spectrometer is separated from the beamline by a 200 μm thick beryllium window. The UHV hosting chamber is equipped with a 4 degrees of freedom ($xyz\theta$) manipulator mounted in vertical position and the sample cooling is obtained by a closed cycle cold finger (18 K at the sample position). The chamber is designed to permit, without breaking the vacuum, the fast introduction and exchange of samples prepared ex situ. It also hosts some basic tools for in situ preparation such as e-gun, ion-gun, scraper, mass spectrometer. Fig. 1 shows a sketch of the experimental set-up, including the analyser. The axis of the analyser lens is at 45° with respect to the incoming photon beam, in the horizontal plane. The energy dispersion within the analyser spheres takes place in the vertical plane.

2.2. Analyser + detector

The hemispherical electrostatic electron energy analyser has been chosen as spectrometer, due to the high resolution that this instrument gives at low kinetic energy and also because this solution allows parallel detection. The analyser consists of a commercial dispersing element (MB Scientific AB [21]) coupled to an electrostatic input lens designed for working with high retarding values [22]. The lens system is composed of seven independent cylindrical electrodes for a total length of 732 mm, with a working distance of 40 mm. The input lens system operates with two schemes with constant linear magnification, $M_l \sim 12$ and $M_l \sim 20$, and retarding factors R (defined as the ratio between the

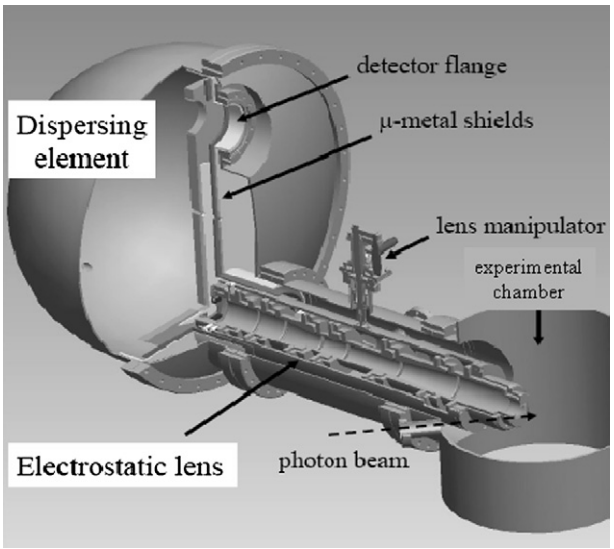

Fig. 1. Sketch of the experimental setup used for the HAXPES experiments at beamline ID16 (ESRF).
Fig. 1. Schéma du montage expérimental utilisé pour les expériences HAXPES sur la ligne ID16 de ESRF.

kinetic energy and the pass energy) ranging from 0.2 to 600. In order to maximize the accepted angle (defined as the maximum photoelectron emission angles transmitted by the input lens into the hemisphere) the lens should work with low angular magnification. Considering the high value of R, the lens is operated with a value of M_l ranging between 10 and 20, to keep the angular magnification less than 3. This value represents a good compromise between the reduction of the field of view in the dispersing direction (due to a high M_l and a small slit height) and the increase in the accepted angle along the non-dispersing direction.With the constraints of a high retarding factor and of a constant linear magnification, the layout of the input lens was first simulated using a ray-tracing code, and then tested experimentally on a prototype. Experimental results agree well with simulations [19,22].

The stability of HV power supplies is a crucial parameter to achieve good energy resolution in HAXPES experiments. For the VOLPE system, we developed a specific power supply architecture, since no commercial unit was providing the desired precision and stability. The high voltage (up to 10 kV) supplied to the analyzer goes through a high voltage divider (HVD) and the divided voltage is measured by a digital voltmeter (DVM) over the 0–1 kV range. Reading the output as close as possible to the analyzer UHV feedthrough, the DVM signal feeds a DC source that corrects the high voltage. Additional power supplies units (Sincrotrone Trieste SY900) float on top of the 10 kV source, making it possible to perform energy scans without modifying the HV output. In such a scheme, the overall stability depends on both the DVM and the HVD. This power supply system has proven to be stable at 10 keV within 27 mV of precision over several days.

The electron analyzer is equipped with a cross delay anode detector. It consists of a 30 mm × 30 mm detector with 0.1 mm spatial resolution [23]. The detector thus permits a parallel acquisition over 300 channels, each of them with an energy width of 3 to 20 meV depending on the pass energy. The detector has been modified to permit floating operation up to 10 kV and equipped with a home made acquisition electronics. The choice of a cross delay anode was motivated by the low dark counts rate of this type of detector which is dominated by the Micro Channel Plates dark counts. For our detectors, dark counts ranges between 2 to 10 counts/s, depending on the voltage that is applied to the MCP.

The performances of the VOLPE setup in terms of energy resolution and count rate has been tested in a dedicated experiment on the ID16 beamline using Au polycrystalline foils as reference samples [19]. Fig. 2 shows the Fermi edge of Au recorded at $h\nu = 5934$ eV and $T = 18$ K, with PE = 20 eV and a slitwidth of 0.4 mm. The spectrum has been acquired in fixed mode i.e. accumulating over the energy range defined by the acceptance of the detector in the dispersive direction, without changing any voltage. The obtained EDC spectrum has been fitted by a linear DOS times a Fermi–Dirac distribution function, convoluted with a Gaussian function. The best fit has been obtained for a Gaussian FWHM of 71 meV which represents the overall instrumental broadening. Alternatively, the energy resolution ΔE has

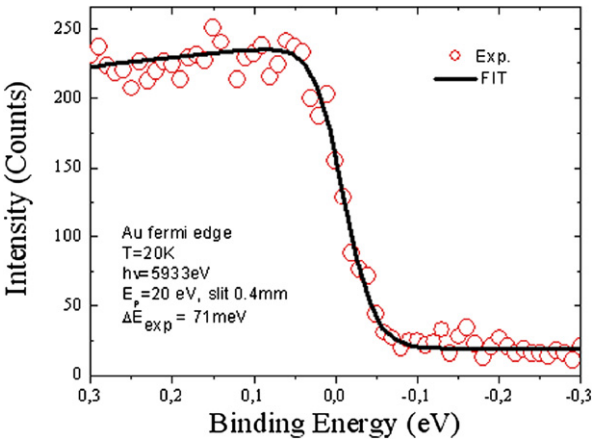

Fig. 2. Au Fermi level (open circles) measured at $h\nu = 5934$ eV and $T = 18$ K in snapshot mode. The acquisition time was 150 minutes and the counts correspond to an integration over 8 mm of detector active area. Solid line: best fit using a Fermi–Dirac function convoluted with a Gaussian of 71 meV FWHM.

Fig. 2. Niveau de Fermi de l'or (symboles) mesuré pour une énergie des photons de 5934 eV à $T = 18$ K dans le mode dit *snapshot*. Le temps d'acquisition était de 150 minutes. La ligne continue est un affinement avec une fonction de Fermi–Dirac convoluée avec une gaussienne d'une largeur à mi-hauteur de 71 meV.

been evaluated by using the formula $\Delta E = 4k_B\sqrt{T_{\text{fit}}^2 - T_{\text{sample}}^2}$, where k_B is the Boltzmann's constant. Taking into account the energy resolution of the photons (≈50 meV), we estimate the analyser energy resolution to be 51 ± 8 meV.

3. Results

3.1. Estimate of HAXPES probing depth and cross section behaviour

Measurements performed in the low energy range showed that the exact value of the escape depth of electrons depends on the electronic configuration, and model calculations estimating the depth sensitivity for kinetic energies above 2 keV are scarce [24,25]. In order to clarify the conditions for the feasibility of future HAXPES experiments and to move into applications of bulk sensitive valence band photoemission, a more accurate and quantitative knowledge of the probing depth is required. Therefore, we have set up a dedicated experiment for determining the effective attenuation length (EAL) of high energy (4–6 keV) electrons via the so-called overlayer method, using wedged overlayers [20]. Four different overlayer samples were chosen in such a way as to cover different classes of materials, namely noble metals (Cu), open 3d shell metals (Co), semiconductors (Ge) and open 4f shell, strongly correlated oxides (Gd_2O_3). The substrate was always a silicon wafer. More details of the experimental set-up can be found in Ref. [20].

We define λ as the thickness of the overlayer that reduces to 1/e the intensity I^s of a core level emission from the substrate, assuming a unitary intensity I_o^s for the bare substrate. Therefore, the intensity of a core level peak from the substrate varies as a function of the overlayer thickness x as $I^s(x) = I_o^s e^{-x/\lambda}$. In the same way, the intensity I of a peak related to the excitation of a core electron in the overlayer will vary as $I(x) = I_o(1 - e^{-x/\lambda})$, I_o being the intensity for an infinite thickness of the overlayer. It is worth underlining that, in both cases, λ expresses a property of the overlayer material. Measuring the bare substrate and a very thick overlayer fixes the values of I_o^s and I_o, thus making λ the only free parameter for a given electron kinetic energy E_k. Experimental data of intensity versus thickness were collected for several core levels and fitted by the above exponential functions. An example is given in Fig. 3, showing three curves obtained measuring the Si-1s emission intensity as a function of the thickness of the Gd_2O_3 overlayer, for 5925, 7500 and 8000 eV photon energy. The results of our analysis are summarized in Fig. 4, which gives an experimental estimate of EAL in different materials for electron kinetic energies between 4 keV and 6 keV. The values that we obtain for Co, Cu and Ge are fairly similar and close to predictions based on the best available models [26,27]. In the case of Gd_2O_3, the values that we obtain for λ are always smaller than for all the other samples and of any available theoretical estimate. Overall, our results confirm that, for $E_k \sim 6$ keV, photoelectrons

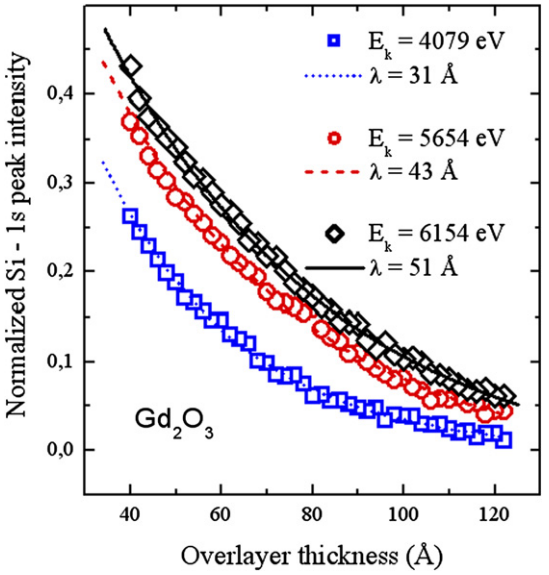

Fig. 3. Normalized Si-1s photoemission intensity measured in fixed mode acquisition (see text). The normalized Si-1s peak intensity is plotted against the Gd_2O_3 overlayer thickness for three different kinetic energies. Lines are obtained by fitting with an exponential decay function.

Fig. 3. Intensité normalisée du pic 1s du Si mesurée en *mode fixe* (voir texte). L'intensité est représentée en fonction de l'épaisseur de la couche de Gd_2O_3 pour trois valeurs de l'énergie cinétique. Les lignes sont des affinements avec un exponentiel décroissant.

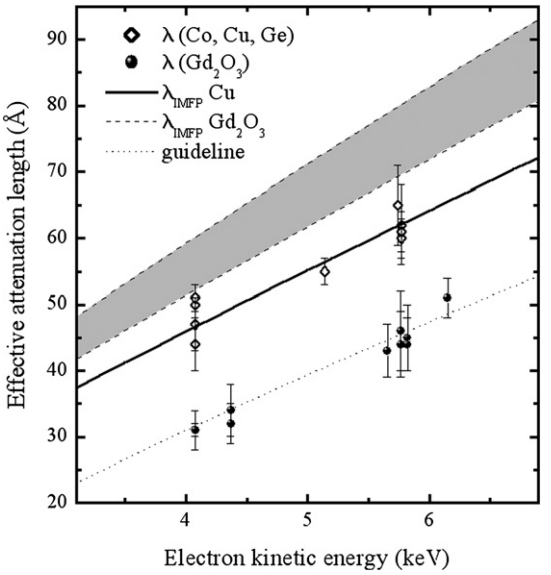

Fig. 4. Graph of the experimental values $\lambda(E_k)$ versus electron kinetic energy. Open diamonds represent experimental values for Co, Cu and Ge, filled circles those for Gd_2O_3. The full line is a calculation of $\lambda(E_k)$ for Cu [26]. The two dashed lines and the encompassed gray area correspond to calculated values for Gd_2O_3, allowing for maximum variation of parameters [24,25]. The thin dotted line is a guide for the eye, obtained by fitting Gd_2O_3 data with a $(E_k)^{0.75}$ dependence.

Fig. 4. Graphique des valeurs expérimentales $\lambda(E_k)$ en fonction de l'énergie cinétique. Les carreaux font référence à Co, Cu et Ge, les cercles à Gd_2O_3. Le trait continu est le résultat d'un calcul pour le Cu [26]. La ligne pointillée est obtenue en approximant les données pour Gd_2O_3 avec une dépendance de type $(E_k)^{0,75}$.

can travel an average distance of 50 to 65 Å before suffering an inelastic collision. The corresponding information depth (defined as the layer thickness from which 95% of the total signal is produced) is of the order of 150–200 Å.

Assuming that the thickness of the surface layer is 1 Å (or 5 Å), the surface contribution at 6 keV is of the order of 2% (respectively, 7%) of the total intensity. At $E_k = 600$ eV, already a high kinetic energy by usual standards, the surface layer contributes 12% of the total intensity if it is 1 Å and 46% if it is 5 Å. The corresponding information depth is 24 Å. We believe that it is important to give explicit values to these parameters in order to quantify the role of high energy photoemission as a probe of the bulk electronic properties of solids. One can also point out that typical capping layers which are used for protecting samples from contamination are 20 to 40 Å thick. In a HAXPES experiment, they will reduce the signal from the underlying sample by less than a factor of two. This implies that protected samples can be measured easily and that in-situ preparation under ultra-high vacuum conditions is no longer a strict requirement for core level photoemission spectroscopy. Also, the signal from buried interfaces and thin films will be more accessible.

The importance of the Photoionisation Cross Section (PCS) is not diminished in the high energy PES with respect to standard PES; for example, we have shown in the section 'Experimental considerations' how the low values of the PCS set strict requirements on the experimental setup. It is important to underline that the reduction of the PCS in the HAXPES regime is not uniform for all the subshell. In fact, as already predicted by calculations [9,18], the reduction of the PCS is more pronounced for shell with high l values; therefore the spectral weight of peaks related to f and d electrons, which are in general very intense in PES, are severely reduced and their intensities are comparable or smaller than those of s and p levels [17]. Besides the relative change of the spectral weights of the different core level peaks, this effect carries important consequences in the photoemission spectra from the valence band (VB). In fact, in the VB

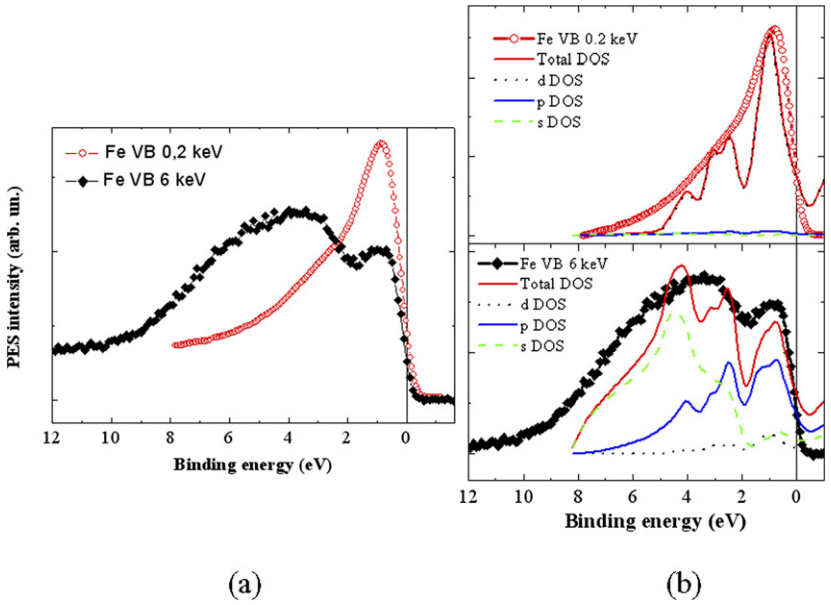

Fig. 5. Panel (a) Photoemission spectra of the Fe valence band recorded with 0.2 (red circles) and 6 keV (black squares) of photon energy. Panel (b) The experimental Fe VB spectra (black circles) are compared with the theoretical curves (red lines) obtained by summing the s (green dashed line), p (blue continuous line) and d (black dotted) contributions weighted for their relative PCS.

Fig. 5. (a) : Spectres de photoémission de la bande de valence du fer mesurés avec des énergies de photon de 0.2 keV (cercles rouges) et 6 keV (carrés noirs). (b) : Comparaison entre données expérimentales (noires) et courbes théoriques (rouges) obtenues en sommant les composantes s (vertes), p (bleues continues) et d (bleues pointillés), chacune pesée par son propre PCS.

region the contributions from states with different symmetry are overlapped in energy and consequently difficult to separate. Large changes in relative cross-sections can be exploited to investigate the sp contribution to the valence state of 3d compounds, where the intensity of the d levels dominate PES spectra. In Fig. 5(a) we show two spectra of the Fe valence band recorded at normal emission from a Fe(001) single crystal prepared by cycles of sputtering and annealing in UHV. The two spectra are taken with photon energies of 0.20 and 6 keV, respectively. The large difference between the two spectra arises only from the change of the relative PCS of the different states of the iron VB. To demonstrate the role of the change of the PCS in modifying the spectrum shape we have performed density functional calculation using the full-potential linearized augmented plane wave technique. We have considered a bulk of iron assuming a lattice parameter of 5.417 a.u. and the PBE version [28] of the generalized gradient approximation of the exchange–correlation potential. The DOS obtained with this method have been convoluted with a Gaussian function of 400 meV of FWHM that accounts for the instrumental broadening. Successively we have weighted the different s, p and d contributions for the relative PCS. The PCS of 4s and 3d shells are tabulated in Refs. [9,18]. Photoemission spectra of the iron VB after an integral background subtraction are compared to calculations in Fig. 5(b). The dramatic change in the iron valence band PES spectrum as a function of the photon energy is explained entirely by the change in the ratio between PCS (3d) and PCS (4s) from 60 at 0.2 keV to 0.1 at 6 keV.

3.2. Metal–insulator transition in transition metal oxides

3.2.1. Metal–insulator transition in V_2O_3

The metal–insulator transition (MIT) is arguably the most-studied open problem in the field of solid-state physics. Such transitions are due to a subtle interplay between various interactions with comparable energy scales, such that the system can be driven from one state to another by a small external parameter, such as the temperature, magnetic field or the composition. Vanadium sesquioxide V_2O_3 (and other vanadates, like VO_2) are the archetypes of the MIT, as described by the Mott–Hubbard theory [1,29]. Despite a gigantic theoretical and experimental effort, MIT in Mott–Hubbard systems is still steeped with controversies. Recent high resolution photoemission experiments using soft X-rays on V_2O_3 in the metallic phase, yield valence band spectra in which the so-called coherent peak is substantially

larger than the incoherent peak, very much unlike the more surface sensitive spectra taken with ultra-violet light [7]. Although we have indications that the true bulk spectra have not been revealed yet, those recent soft X-ray spectra already reveal that the bulk material has a much more pronounced coherent peak than can be reproduced by one the most sophisticated theoretical approaches to calculate realistic spectra for correlated systems, namely the LDA+DMFT method.

We addressed these questions by using HAXPES at ≈5.95 keV of photon energy on a pure vanadium sesquioxide single crystal, by measuring core level and valence band spectra. V_2O_3 presents a MIT Mott-like transition as a function of both temperature and pressure (or doping); pure V_2O_3 crystallizes in the α-corundum structure at room temperature and undergoes a first order transition at 150 K passing from the paramagnetic metallic (PM) phase to the antiferromagnetic insulating (AFI) one, with monoclinic structure. Across the MIT one observes a change in resistivity of several orders of magnitude and a large volume increase that, in pure V_2O_3, makes the MIT destructive, resulting in some cases to a pulverization of the sample. Fig. 6 shows the V $2p_{3/2}$ core level spectra in the PM and the AFI phase. In the PM spectrum, a clear satellite appears at 512.4 eV ($2p_{3/2}$) of binding energy. The main features of the spectra are in agreement with previous data obtained on $V_{1.98}Cr_{0.02}O_3$ in the HAXPES regime [30]. We underline that the fine structure observed in the spectra of Fig. 6, with a clear energy separation between main peaks and satellite intensities, is practically absent in surface sensitive PES, including conventional XPS [31,32]. When crossing the MIT, an important change of spectral weight is observed, leaving the main peak with almost no satellite structure. Similar features are observed for the $2p_{1/2}$ and 3p core levels. The presence of shake-down satellites is caused by the improved screening on the core hole, which creates a new impurity state near E_f with an additional electron in the final state of the photoionization process [11,12,30]. Recently, the presence and the evolution of shake-down satellites in the 4d core level of ruthenates has been explained in relation to the properties of a Mott–Hubbard system via a DMFT calculation [33]. In Fig. 7 we present valence band photoemission results: a well defined quasiparticle peak is observed in the metallic phase [7]. The comparison between the PM and AFI phase spectra reveals the complete disappearance of the coherent peak, with the spectral weight transferred in a broad band extending from 0.5 to 2.0 eV, and the opening of a gap which we estimate of 220 ± 20 meV at the E_F position. It is important to underline that a gap, of the same order of magnitude as that of Fig. 7, opens for both the cleaved samples, and that in both cases a transfer of spectral weight is visible in the core level after the MIT occurs. Scraped samples do not display any gap opening, and intensity near E_F is practically absent. the DMFT calculation are in overall good agreement with the HAXPES valence band results and have been used to estimate the Hubbard U correlation term [34]. Remarkably, the presence of a well defined satellites is directly related to a well defined coherent peak near E_f. Shake down features, so clearly observed in HAXPES, appear at best as weak shoulders in lower energy PES experiments, the main difference between the two experiments being the probing depth. If one defines the information depth as the thickness from which 90% of the PES signal originates, HAXPES reaches 150–200 Å at 6 keV kinetic energy, to be compared with 5–10 Å and <30 Å of UPS and XPS regimes, respectively [20]. The increased depth sensitivity argument nicely explains both the appearance of the new shake down satellites in the core level and the presence of the coherent peaks near E_f. The present observation does not imply that the same correspondence exists in all transition metal oxides presenting a shake down satellite, but sets, in the case of V_2O_3, a firm experimental basis for a complete theoretical description.

3.3. Bilayer manganites

Manganites comprise a large class of strongly-correlated magnetic materials that exhibit the colossal magnetoresistance (CMR) effect, as well as, in some cases, half-metallic ferromagnetism [35]. A particular set of samples which has been investigated intensively are the layered compounds ($La_{2-2x}Sr_{1+2x}Mn_2O_7$) which have been shown to present a particularly large CMR effect [36]. The layered nature of these material promotes a strong anisotropy that induces a quasi two-dimensional electronic behavior and is responsible for their peculiar properties compared to the three-dimensional parent compounds [37]. For $x \sim 0.4$, in particular, recent experiments claim a strong difference between the outermost Mn–O bilayers and the bulk of the material: below the Curie temperature (T_C), the surface would still have an insulating behavior while the interior of the system would behave as a metallic-ferromagnet [38]. The $La_{1.2}Sr_{1.8}Mn_2O_7$ (LSMO) sample is a ferromagnetic metal below the transition temperature T_C of about 120 K, changing to a paramagnetic insulator above T_C. The crystal structure is derived from the perovskite structure by interleaving double blocks of rocksalt structure, (La,Sr)O, between two perovskite sheets [39]. PES experiments with

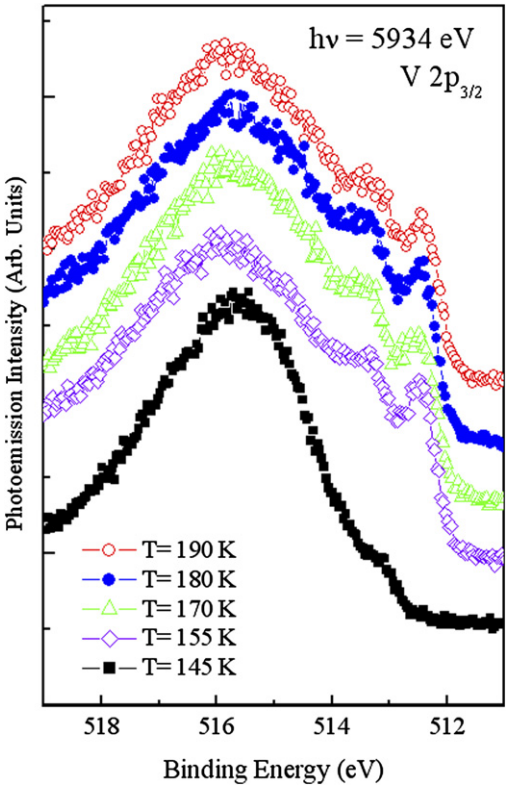

Fig. 6. Temperature dependence of the V $2p_{3/2}$ core level spectra, measured at $h\nu$ = 5934 eV in the PM and the AFI phase. Spectra have been normalized by a multiplication factor in order to match the intensity either side of the peaks and shifted along the intensity axis for better comparison.The energy separation between the well screened features and the main lines, is 3.25 ± 0.05 eV.

Fig. 6. Dépendance en température des niveaux de coeur 2p du V à travers la transition PM-AFI (5934 eV de photon). Les spectres ont été normalisés en dehors des pics et décelés en verticale pour une meilleure visualisation. La séparation en énergie entre la structure well screened et le pic principale est de $3,25 \pm 0,05$ eV.

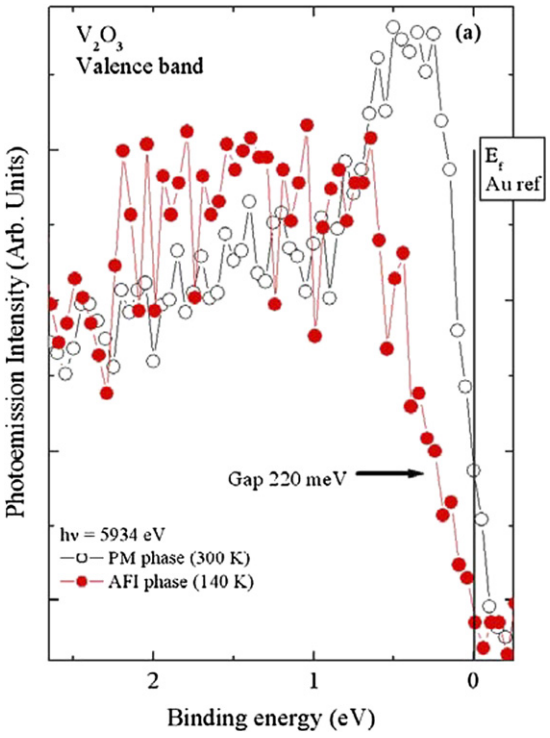

Fig. 7. HAXPES Valence band spectra in the PM (white circles) and AFI (filled circles) phase. Raw data with no background subtraction. Spectra reveal the complete disappearance of the coherent peak and the opening of a gap of 220 ± 20 meV in the AFI phase.

Fig. 7. Bande de valence HAXPES du V_2O_3 dans la phase PM (cercles vides) et AFI (cercles remplis). On observe la disparition du pic cohérent et l'ouverture d'un gap de 220 ± 20 meV dans la phase AFI.

about 1.5 keV photons hardly show any difference between spectra collected above and below the transition temperature [40].

In order to obtain spectral information on the MIT we performed HAXPES experiments varying the temperature across T_C on LSMO single crystals prepared by the floating zone method [41] at the Argonne National Laboratory (USA), either cleaved in air or fractured in vacuum. As a function of temperature, we observed differences in spectral shapes and peak positions, both in core level and in valence band spectra, revealing changes in the bulk electronic properties [42]. In particular O 1s spectra measured at temperatures lower than T_C are more asymmetric, with a higher intensity tail toward the high binding energy side, suggesting a metallic behavior. Also, the peak shifts by approximately 100 meV toward a lower binding energy compared to the spectrum collected at temperatures higher than T_C. These observations are indicative of the MIT, in analogy with the results obtained at fixed temperature by varying the doping level in cubic perovskite thin films [12]. It is worth noticing that we did not observe any peak shift in other core levels, such as Mn 2p (see below) and Sr 3d (not shown). On the other hand, one of the two components of the Mn 3s doublet is shifted in energy by crossing T_C, resulting in a narrowing of the splitting between the two 3s components (Δ_{3s}) in the ferromagnetic phase. This can be seen in Fig. 8 where Mn 3s spectra taken at $T = 300$ K

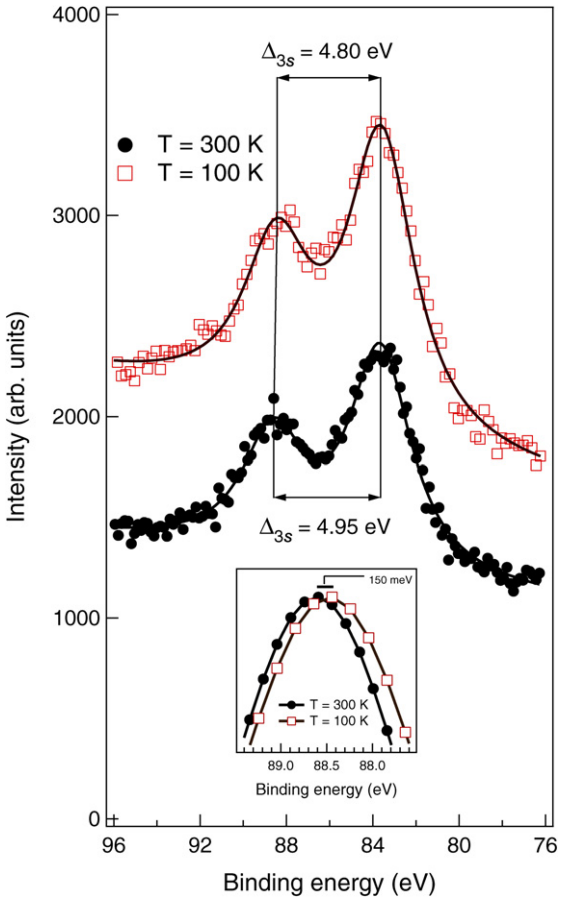

Fig. 8. Mn 3s spectra taken at $T = 300$ K (solid circles), i.e. above T_C, and at $T = 100$ K (open squares), i.e. below T_C. Solid lines are the results of best fits with Voigt functions. The inset in the bottom part shows the Voigt components used to represent the peak at higher binding energy for the two temperatures, outlining the shift of about 150 meV in the relative peak position.

Fig. 8. Spectres 3s du Mn mesurés à $T = 300$ K (au dessus de T_C, cercles) et à $T = 100$ K (au dessous de T_C, carrés). Les traits continus sont des affinements avec une fonction de Voigt. Les composantes des fonctions de Voigt utilisées pour le pic à plus haute énergie de liaison sont comparées en bas de la figure, montrant qu'il y a un décalage de 150 meV dans la position du pic entre les deux températures.

(solid circles) and $T = 100$ K (open squares) are shown. Superimposed to the experimental results (symbols) are the best fits with Voigt functions (solid lines) plus integral background, where the width of the Gaussian component has been fixed to the experimental resolution, and the Lorentzian full width at half maximum has been set equal for both 3s components. The decrease in the doublet splitting (Δ_{3s}) by lowering T amounts to 150 meV, and is induced by a shift of the component at higher binding energy. This is best visible in the inset in the bottom part of Fig. 8 where the Voigt component used for representing this peak is overlapped after intensity normalization. The component at lower binding energy, on the other hand, does not shift its energy position at the two temperatures. Fig. 9 shows the change in spectral shape from above (solid circles) to below (open squares) T_C of the Mn $2p_{3/2}$ core level [Fig. 9(a)] and close to the Fermi level [Fig. 9(b)]. At low temperature, the Mn $2p_{3/2}$ curve shows a pronounced shoulder at around 638.5 eV on the low binding energy side of the peak. This feature, prominent in the HAXPES spectrum of the metallic phase but hard to observe in conventional PES spectra, is similar to the structure reported in three-dimensional perovskite manganites by Horiba et al. [11]. These authors interpreted the extra feature as a well-screened final state, related to the metallic and magnetic properties of the sample [43]. In Fig. 9(b) the spectrum acquired close to the Fermi level at low temperature (open squares), is compared with that collected at higher temperature (solid circles): an increased intensity at approximately 0.4 eV of binding energy is visible in the spectrum measured below T_C.

Our bulk sensitive measurements outline the changes in the electronic properties when crossing T_C. In particular, the shift of the O 1s peak toward lower binding energies [42] can be interpreted as due to a charge transfer from

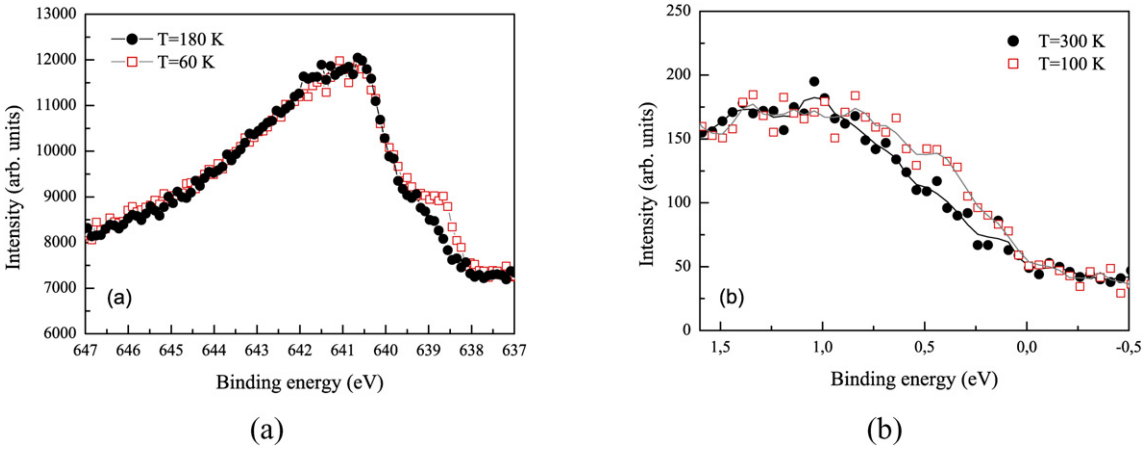

Fig. 9. (a) Mn $2p_{3/2}$ spectra at $T = 180$ K (solid circles) and $T = 60$ K (open squares). (b) Intensity close to the Fermi level at $T = 300$ K (solid circles) and $T = 100$ K (open squares). Lines are a guide to the eye.

Fig. 9. (a) : Spectres du Mn $2p_{3/2}$ à $T = 180$ K (cercles) et $T = 60$ K (carrés). (b) : Intensité au voisinage du niveau de Fermi à $T = 180$ K (cercles) et $T = 60$ K (carrés). Les traits représentent seulement un aide à la visualisation.

Mn to O. In this simple picture, one should observe a concomitant increase of the Mn valence, or an increase in the Mn^{4+}/Mn^{3+} ratio. This is exactly what can be inferred from the analysis of the Mn 3s spectra (Fig. 8): in fact, a lower Δ_{3s} can be related to an increased Mn valence, as it was suggested by the results of Galakhov et al. [44] and Mannella et al. [45]. Such change in Mn valence, related to a charge transfer toward oxygen, may be the result of a structural modification accompanying the MIT transition: an enhanced distortion (namely an increased bond length in one of the two Mn–O apical bonds) accompanying charge delocalization (i.e., metallic state) has indeed been reported for layered manganites, and interpreted as the response of the system to the magnetic ordering [41,46]. The vertical elongation of the Mn–O bond is also consistent with the observation of a change in the intensity close to the Fermi edge with temperature [see Fig. 9(b)]. The bump around 0.4 eV of binding energy is commonly interpreted as the Mn e_g band, and, in our measurements, it is observed to shift toward the Fermi level at low temperature. An in-plane structural contraction would lead to a configuration where the vertical $3z^2 - r^2$ orbital has lower energy and is prevalently occupied, leading to a narrower e_g band, which comes closer to the Fermi edge [47], precisely as observed in our spectra [see Fig. 9(b)]. Note that, as in lower energy photoemission [40], the intensity at the Fermi level remains vanishingly small, both below and above T_C, and in particular no states at E_F, such as a quasiparticle peaks, can be detected. Therefore, it appears that the concomitant observation in HAXPES of a core level extra peak and of a quasiparticle peak at the Fermi edge, experimentally demonstrated in some complex materials such as V_2O_3 (see previous subsection), might not be a general feature of transition metal oxides. In our LSMO layered sample the intense shoulder in the Mn $2p_{3/2}$ peak is linked to the metallic and magnetic phase of the sample, but apparently has no relation with an extra density of states at the Fermi level. Our results agree rather well with the model of van Veenendaal, which associates the extra peak to non-local screening [48]. Within this approach, cluster calculations mimic core level spectra and relate the observation of low-binding energy features not to the existence of a quasiparticle state at the Fermi level but to the presence of non-local screening channels, whose relative importance depends on the electronic and magnetic properties of the sample. According to this picture, the enhanced intensity of the peak at low binding energies observed in our experiment is due to the increased hopping probability at low temperature and can be seen as a benchmark of, for instance, an increased magnetic ordering.

4. Conclusions

In summary, our results demonstrate that high resolution HAXPES can be performed at high brilliance/high resolution beamlines of third generation synchrotron radiation sources. Results for V_2O_3 and *quasi* two-dimensional bilayered manganites confirm that HAXPES experiments may reveal the details of the MIT transition, with clear signatures of the metallic/insulating character. In spite of the more challenging experimental conditions of HAXPES

with respect to conventional XPS, we anticipate potential applications to technological samples in buried interfaces, thanks to the larger probing depths and to the much relaxed vacuum and surface preparation requirements.

Acknowledgements

We are grateful to Prof. Yves Baer for his enthusiastic support to this project. We thank Prof. M. Grioni (EPFL, Switzerland) and Prof. H. Tjeng (University of Köln, Germany) for fruitful discussion, Dr. V. Bellini for allowing us to use his calculations and the ID16 staff (Dr. G. Monaco, Dr. G. Vanko and Dr. S. Huotari) for support during the beamtime. Technical assistance from C. Henriquet (ID16) is gratefully acknowledged. This work received financial support from the European Community under the RTD contract HPRI-CT-2001-50032.

References

[1] M. Imada, A. Fujimori, Y. Tokura, Rev. Mod. Phys. 70 (1998) 1039;
R.J. Birgenau, M.A. Kastner, Science 288 (2000) 437.
[2] C. Laubschat, E. Weschke, C. Holtz, M. Domke, O. Strebel, G. Kaindl, Phys. Rev. Lett. 65 (1990) 1639.
[3] Yu. Kucherenko, S.L. Molodtsov, M. Heber, C. Laubschat, Phys. Rev. B 66 (2002) 155116.
[4] A. Sekiyama, T. Iwasaki, K. Matsuda, Y. Saitoh, Y. Onuki, S. Suga, Nature 403 (2000) 396.
[5] T. Claesson, M. Månsson, C. Dallera, F. Venturini, C. De Nadaï, N.B. Brookes, O. Tjernberg, Phys. Rev. Lett. 93 (2004) 136402.
[6] J.-H. Park, L.H. Tjeng, A. Tanaka, J.W. Allen, C.T. Chen, P. Metcalf, J.M. Honig, F.M.F. de Groot, G.A. Sawatzky, Phys. Rev. B 61 (2000) 11506.
[7] S.-K. Mo, J.D. Denlinger, H.-D. Kim, J.-H. Park, J.W. Allen, A. Sekiyama, A. Yamasaki, K. Kadono, S. Suga, Y. Saitoh, T. Muro, P. Metcalf, G. Keller, K. Held, V. Eyert, V.I. Anisimov, D. Vollhardt, Phys. Rev. Lett. 90 (2003) 186403.
[8] I. Lindau, P. Pianetta, S. Doniach, F. Spicer, Nature 250 (1974) 214.
[9] J.J. Yeh, I. Lindau, Atomic Data and Nuclear Data Tables 32 (1985) 1.
[10] See Nucl. Instrum. Meth. A 547 (2005) 1–238, issue dedicated to hard X-ray photoemission spectroscopy.
[11] K. Horiba, M. Taguchi, A. Chainani, Y. Takata, E. Ikenaga, D. Miwa, Y. Nishino, K. Tamasaku, M. Awaji, A. Takeuchi, M. Yabashi, H. Namatame, M. Taniguchi, H. Kumigashira, M. Oshima, M. Lippmaa, M. Kawasaki, H. Koinuma, K. Kobayashi, T. Ishikawa, S. Shin, Phys. Rev. Lett. 93 (2004) 236401.
[12] K. Horiba, M. Taguchi, N. Kamamura, K. Yamamoto, A. Chainani, Y. Takata, E. Ikenaga, H. Namatame, M. Taniguchi, M. Awaji, A. Takeuchi, D. Miwa, Y. Nishino, K. Tamasaku, T. Ishikawa, H. Kumigashira, M. Oshima, M. Lippmaa, M. Kawasaki, H. Koinuma, K. Kobayashi, S. Shin, J. Electron Spectrosc. Relat. Phenom. 557 (2005) 144–147.
[13] K. Kobayashi, M. Yabashi, Y. Takata, T. Tokushima, S. Shin, K. Tamasaku, D. Miwa, T. Ishikawa, H. Nohira, T. Hattori, Y. Sugita, O. Nakatsuka, A. Sakai, S. Zaima, Appl. Phys. Lett. 83 (2003) 1005.
[14] H. Sato, K. Shimada, M. Arita, K. Hiraoka, K. Kojima, Y. Takeda, K. Yoshikawa, M. Sawada, M. Nakatake, H. Namatame, M. Taniguchi, Y. Takata, E. Ikenaga, S. Shin, K. Kobayashi, K. Tamasaku, Y. Nishino, D. Miwa, M. Yabashi, T. Ishikawa, Phys. Rev. Lett. 93 (2004) 246404.
[15] A. Chainani, T. Yokoya, Y. Takata, K. Tamasaku, M. Taguchi, T. Shimojima, N. Kamakura, K. Horiba, S. Tsuda, S. Shin, D. Miwa, Y. Nishino, T. Ishikawa, M. Yabashi, K. Kobayashi, H. Namatame, M. Taniguchi, K. Takada, T. Sasaki, H. Sakurai, E. Takayama-Muromachi, Phys. Rev. B 69 (2004) 180508(R).
[16] C. Dallera, L. Duò, L. Braicovich, G. Panaccione, G. Paolicelli, B. Cowie, J. Zegenhagen, Appl. Phys. Lett. 85 (2004) 4532.
[17] S. Thiess, C. Kunz, B.C.C. Cowie, T.-L. Lee, M. Renier, J. Zegenhagen, Solid State Commun. 132 (2004) 589.
[18] J.H. Scofield, Theoretical photoionisation cross section from 1 to 1500 keV, LLNL Report UCRL-51326, 1973, available at http://www-pat.llnl.gov/Research/scattering/RTAB.html, by L. Kissel.
[19] P. Torelli, M. Sacchi, G. Cautero, M. Cautero, B. Krastanov, P. Lacovig, P. Pittana, R. Sergo, R. Tommasini, A. Fondacaro, F. Offi, G. Paolicelli, G. Stefani, M. Grioni, R. Verbeni, G. Monaco, G. Panaccione, Rev. Sci. Instrum. 76 (2005) 023909.
[20] M. Sacchi, F. Offi, P. Torelli, A. Fondacaro, C. Spezzani, M. Cautero, G. Cautero, S. Huotari, M. Grioni, R. Delaunay, M. Fabrizioli, G. Vankô, G. Monaco, G. Paolicelli, G. Stefani, G. Panaccione, Phys. Rev. B 71 (2005) 155117.
[21] MBscientific, Sweden, http://www.mbscientific.se.
[22] F. Offi, A. Fondacaro, G. Paolicelli, A. De Luisa, G. Stefani, Nucl. Instrum. Meth. A 550 (2005) 454.
[23] J.V. Vallerga, O.H.W. Siegmund, Nucl. Instr. Meth. Phys. Res. A 442 (2000) 337.
[24] M.P. Seah, I.S. Gilmore, S.J. Spencer, J. Vac. Sci. Technol. A 18 (2000) 1083;
M.P. Seah, I.S. Gilmore, S.J. Spencer, J. Electron Spectrosc. Relat. Phenom. 120 (2001) 93.
[25] S. Tanuma, C.J. Powell, D.R. Penn, Surf. Interface Anal. 35 (2003) 268.
[26] Calculated values of the IMFP up to 10 keV can be found, only for a few selected elements, at the NIST website http://www.nist.gov/srd/nist71.htm;
See also C.J. Powell, A. Jablonski, J. Phys. Chem. Ref. Data 28 (1999) 19;
A. Jablonski, F. Salvat, C.J. Powell, NIST Electron Elastic-Scattering Cross Section Database, version 3.0, National Institute of Standards and Technology, 2002.
[27] P.J. Cumpson, M.P. Seah, Surf. Interface Anal. 25 (1997);
See also http://www.lasurface.com/IMFP/Ag_IMFP_1.htm.

[28] J.P. Perdew, K. Burke, M. Ernzerhof, Phys. Rev. Lett. 77 (1996) 3865.
[29] P.A. Cox, Transition Metal Oxides, Clarendon Press, Oxford, 1992.
[30] M. Taguchi, A. Chainani, N. Kamakura, K. Horiba, Y. Takata, M. Yabashi, K. Tamasaku, Y. Nishino, D. Miwa, T. Ishikawa, S. Shin, E. Ikenaga, T. Yokoya, K. Kobayashi, T. Mochiku, K. Hirata, K. Motoya, Phys. Rev. B 71 (2005) 155102.
[31] K.E. Smith, V.E. Heinrich, Phys. Rev. B 50 (1994) 1382.
[32] D.S. Toledano, P. Metcalf, V. Heinrich, Surf. Science 449 (2000) 19.
[33] H.-D. Kim, H.-J. Noh, K.H. Kim, S.-J. Oh, Phys. Rev. Lett. 93 (2004) 126404.
[34] G. Panaccione, M. Altarelli, A. Fondacaro, A. Georges, S. Huotari, P. Lacovig, A. Lichtenstein, P. Metcalf, G. Monaco, F. Offi, L. Paolasini, A. Poteryaev, M. Sacchi, O. Tjernberg, Phys. Rev. Lett. 97 (2006) 116401.
[35] See, for instance, M.B. Salamon, M. Jaime, Rev. Mod. Phys. 73 (2001) 583, and references cited therein.
[36] Y. Moritomo, A. Asamitsu, H. Kuwahara, Y. Tokura, Nature 380 (1996) 141.
[37] H.M. Rønnow, Ch. Renner, G. Aeppli, T. Kimura, Y. Tokura, Nature 440 (2006) 1025.
[38] J.W. Freeland, K.E. Gray, L. Ozyuzer, P. Berghuis, E. Badica, J. Kavich, H. Zheng, J.F. Mitchell, Nature Mater. 4 (2005) 62.
[39] J.F. Mitchell, D.N. Argyriou, A. Berger, K.E. Gray, R. Osborn, U. Welp, J. Phys. Chem. B 105 (2001) 10731.
[40] J.-Y. Son, T. Mizokawa, J.W. Quilty, S. Hirata, K. Takubo, T. Kimura, Y. Tokura, Phys. Rev. B 70 (2004) 012411.
[41] J.F. Mitchell, D.N. Argyriou, J.D. Jorgensen, D.G. Hinks, C.D. Potter, S.D. Bader, Phys. Rev. B 55 (1997) 63.
[42] F. Offi, P. Torelli, M. Sacchi, P. Lacovig, A. Fondacaro, G. Paolicelli, S. Huotari, G. Monaco, C.S. Fadley, J.F. Mitchell, G. Stefani, G. Panaccione, Phys. Rev. B 75 (2007) 01422.
[43] H. Tanaka, Y. Takata, K. Horiba, M. Taguchi, A. Chainani, S. Shin, D. Miwa, K. Tamasaku, Y. Nishino, T. Ishikawa, E. Ikenaga, M. Awaji, A. Takeuchi, T. Kawai, K. Kobayashi, Phys. Rev. B 73 (2006) 094403.
[44] V.R. Galakhov, M. Demeter, S. Bartkowski, M. Neumann, N.A. Ovechkina, E.Z. Kurmaev, N.I. Lobachevskaya, Ya.M. Mukowskii, J. Mitchell, D.L. Ederer, Phys. Rev. B 65 (2002) 113102.
[45] N. Mannella, A. Rosenhahn, C.H. Booth, S. Marchesini, B.S. Mun, S.-H. Yang, K. Ibrahim, Y. Tomioka, C.S. Fadley, Phys. Rev. Lett. 92 (2004) 166401.
[46] M. Medarde, J.F. Mitchell, J.E. Millburn, S. Short, J.D. Jorgensen, Phys. Rev. Lett. 83 (1999) 1223.
[47] T. Kimura, Y. Tokura, Annu. Rev. Mater. Sci. 30 (2000) 451.
[48] M. van Veenendaal, Phys. Rev. B 74 (2006) 085118.